*Short Communication*

# High-performance $Sm_2Co_{17}$ Based Alloy with Enhanced Magnetic Properties and Improved Corrosion Resistance

*Jinting Li, Minxiang Pan*[*]*, Yundan Yu, Hongliang Ge, Qiong Wu*[*]*

Magnetism key laboratory of Zhejiang Province, China Jiliang University, Hangzhou 310018, China
[*]E-mail: panminxiang@cjlu.edu.cn (Minxiang Pan); wuqiong@cjlu.edu.cn (Qiong Wu)

The magnetic properties, microstructures and corrosion resistance of $Sm_2Co_{17}$ based sintered permanent magnets with the nominal composition $Sm(Co_{bal}Fe_{0.125}Cu_{0.08}Zr_{0.06})_{7.4}$ have been systematically investigated. The $Sm_2Co_{17}$ based magnets were prepared by a traditional powder metallurgy method, where the techniques of making powder were ball-milling and jet-milling, respectively. An enhanced magnetic properties has been obtained for the magnet made of jet-milling powder, where the intrinsic coercivity $H_{cj}$ increases from 2270 to 2879 kA/m, the maximum magnetic energy product $(BH)_{max}$ from 217 to 235 kJ/m$^3$ with a small decrease in remanence $B_r$ only. Besides, a remarkably improvement in electrochemical stability and corrosion resistance for the magnet with the jet-milling powder, which is mainly attributed to the magnet obtains a uniform continuous cellular structure with the smaller cell size and the homogeneous cell boundary phase.

## 1. INTRODUCTION

Among various rare-earth sintered magnets, the precipitation-hardened $Sm_2(Co, Fe, Cu, Zr)_{17}$ sintered permanent magnets have attracted a lot of attention due to its distinguished high temperature magnetic properties, excellent corrosion resistance and oxidation resistance [1-4]. These $Sm_2Co_{17}$ sintered permanent magnet is mainly composed of the rhombohedral $Sm_2Co_{17}$ (2:17R) cell phase and the hexagonal $SmCo_5$ (1:5H) cell boundary phase, while the Zr-rich platelets (Z-phase) is running across the cells and cell boundaries phases [5,6]. In recent years, many efforts have been devoted to improve the magnetic properties and high temperature characteristics based on the $Sm_2(Co, Fe, Cu, Zr)_{17}$ magnets [7,8], most of these researches are based on the adding or substituting elements for Cu, Fe and Zr, thus led to the enhancement of magnetic properties for the $Sm_2(Co, Fe, Cu, Zr)_{17}$ magnets

[7,8]. It is well known that the jet-milling technique is always to pulverize powders for the NdFeB alloys, while the ball-milling is used to make $Sm_2(Co, Fe, Cu, Zr)_{17}$ magnetic powders [9-11].

Until now, the jet-milling technique, which was used to make $Sm_2(Co, Fe, Cu, Zr)_{17}$ magnetic powders, has not been systematically reported. In this work, the comparison between the magnetic properties, microstructures and corrosion resistance of $Sm_2Co_{17}$ based sintered permanent magnets prepared by ball-milling powder and jet-milling powder were systematically investigated. Meanwhile, the temperature dependence of magnetic properties for the $Sm_2Co_{17}$ based magnets made by ball-milling powder and jet-milling powder was also discussed in detail.

## 2. EXPERIMENTAL PART

The magnets investigated in this paper were fabricated using a traditional powder metallurgy method. About 10 kg of the alloy with a nominal composition of $Sm(Co_{bal}Fe_{0.125}Cu_{0.08}Zr_{0.06})_{7.4}$ were made from high purity elements by induction melting furnace, and then the techniques of making powder were ball-milling and jet-milling, respectively. The degassed powder compaction were sintered at 1200-1220 °C for 1 h and then homogenized at 1150-1180 °C for 1.5 h. The subsequent aging was at 800~860 °C for 10 h, followed cooling to 400 °C at a rate of 0.8 °C/min, aging at 400 °C for 5 h and finally quenching to room temperature by water. Meanwhile, the magnets made of ball-milling and jet-milling hereafter designated as type-A magnet and type-B magnet, respectively.

The phase constitutions of the type-A and type-B magnets were examined by X-ray diffraction (XRD) using Cu $K_\alpha$ radiation. The magnetic properties of the type-A and type-B magnets with the size of $\Phi10*10$ mm were accomplished by the Pulsed Field Magnetometer (PFM). The microstructural and phase analysis were investigated by FEI Technai F20 transmission electron microscope (TEM). The polarization curves were measured by the PARSTAT 2273 advance electrochemical system in 2.5 wt.% NaCl aqueous solution with the scan rate of 2 mV/s along the direction from the negative potential to the positive one. Each measurement was performed using two electrode cell consisting of $Sm_2Co_{17}$ based magnets working electrode and Pt counter electrode. Accelerated corrosion test was performed by placing cubic samples (10mm*10mm*10mm) in 120°C, 2 bar and 100% relative humid atmosphere for 24, 48, 72 and 96 h, respectively. The mass losses of the accelerated corrosion test were measured weighing the sample before and after the accelerated corrosion test with removing the corrosion products from the sample surfaces by using the microbalance.

## 3. RESULTS AND DISCUSSION

Figure 1 shows the demagnetization curves of the type-A and type-B magnets at room temperature. Meanwhile, the hysteresis loop of the magnets obtained by PFM were also shown. As shown in Fig.1, the corresponding properties of the type-A magnet are: the remanence $B_r = 1.11$ T, the intrinsic coercivity $H_{cj} = 2270$ kA/m, and the maximum magnetic energy product $(BH)_{max} = 217$ kJ/m$^3$, while that of the type-B magnet are: The remanence $B_r = 1.08$ T, the intrinsic coercivity $H_{cj} = 2879$

kA/m, and the maximum magnetic energy product $(BH)_{max}$ = 235 kJ/m$^3$. Figure 2 gives further information about the temperature dependence of the $B_r$, $H_{cj}$ and $(BH)_{max}$ of the type-A and type-B magnets.
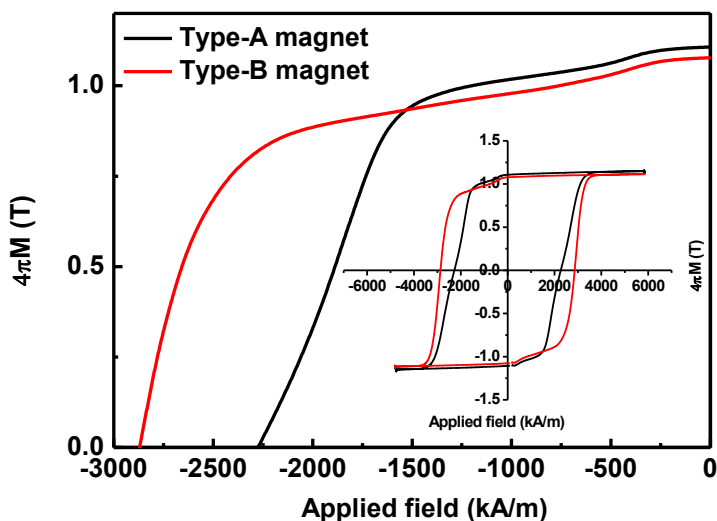


**Figure 1.** Demagnetization curves of the type-A and type-B magnets at room temperature. Insets: the hysteresis loop of the magnets obtained by PFM were also shown.

With the increase of the temperature, two magnets show a decrease of the magnetic properties. As the temperature increases from 295 K up to 448 K, $B_r$ reduces from 1.11 T to 0.99 T, $H_{cj}$ from 2270 kA/m to 1651 kA/m, and $(BH)_{max}$ from 217 kJ/m$^3$ to 175 kJ/m$^3$ for the type-A magnet, while $B_r$ reduces from 1.08 T to 0.97 T, $H_{cj}$ from 2879 kA/m to 2154 kA/m, and $(BH)_{max}$ from 235 kJ/m$^3$ to 205 kJ/m$^3$ for the type-B magnet. Furthermore, the temperature coefficient of coercivity between the 295 K and 448 K for the type-A and type-B magnets is -0.178%/K and -0.164%/K, respectively.
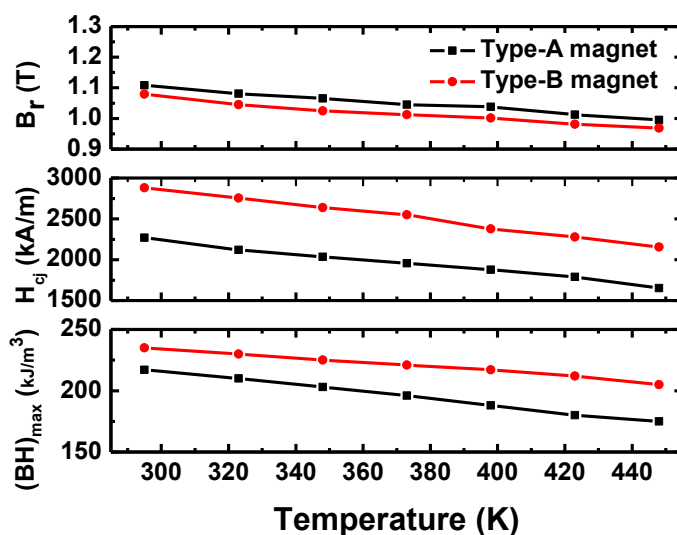


**Figure 2.** Temperature dependence of $B_r$, $H_{cj}$, $(BH)_{max}$ of the type-A and type-B magnets, respectively.
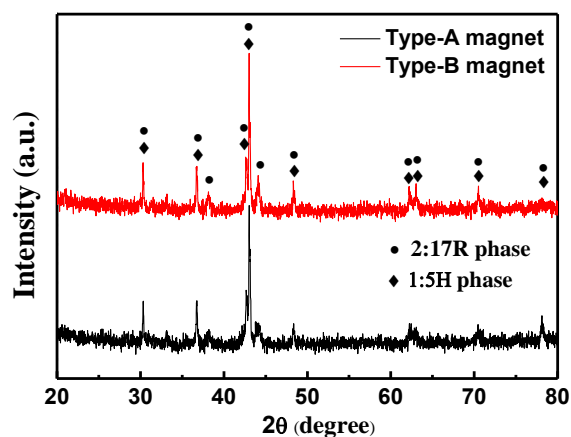
**Figure 3.** X-ray diffraction patterns of the type-A and type-B magnets.

In conclusion, the magnet that is made by jet-milling led to the higher magnetic properties and as a good candidate for high temperature applications, compared to the magnet is made by ball-milling.

In order to investigate phase structure difference between the type-A and B magnets, the XRD patterns of the type-A and B magnets were measured, as shown in Fig. 3. It can be seen that the two samples are almost the same, containing mainly of two phases: rhombohedral $Th_2Zn_{17}$-type (2:17 R) and $CaCu_5$-type phase (1:5 H).
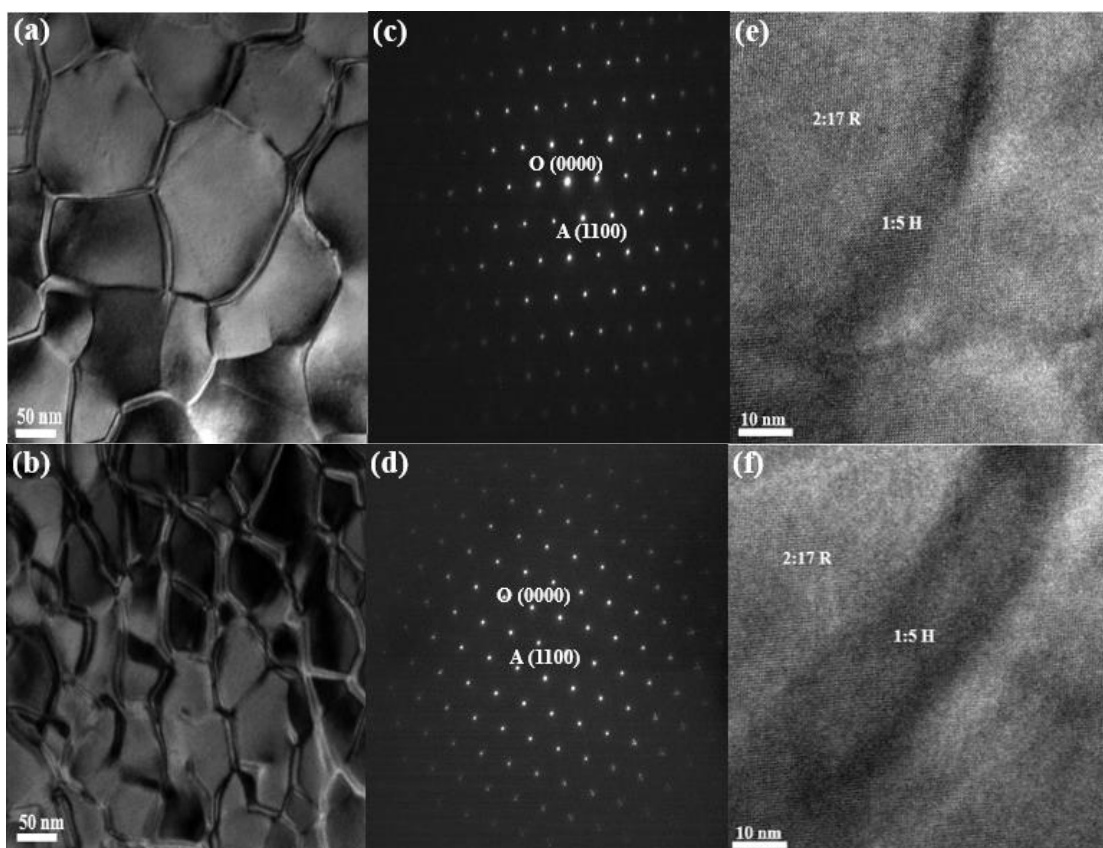


**Figure 4.** TEM/HRTEM images and SAED patterns along $[001]_{2:17R}$ zone axis of the type-A and type-B magnets.

To further investigate the reason that cause the type-A and type-B magnets show such a huge difference on magnetic properties only under the premise of different pulverizing powder technique, the detailed microstructure analysis were investigated by the TEM/HRTEM equipped with selected area electron diffraction (SAED) technique. As shown in the Figs. 4 (a) and (b), the type-A and type-B magnets both demonstrated the cellular structure. The average cell size for the type-A magnet is 160 nm, while the average cell size for the type-B magnet is 70 nm. Furthermore, the Type-B magnet obtained a uniform size of cell and the boundaries are homogeneous and continuous, compared to the Type-A magnet with ununiformed size of cell. Figs. 4 (c) and (d) present the SAED patterns along $[001]_{2:17R}$ zone axis of the type-A and type-B magnets, which are the superposition of the diffraction patterns of the 2:17R cell and 1:5H cell boundary phase, respectively. This result is good consistent with the previous results of XRD that no other phase was observed and previous reports on the $Sm(CoFeCuZr)_z$ magnets [12]. Figs. 4 (e) and (f) show the HRTEM graphs of the cell boundary for the type-A and type-B magnets, respectively. By comparing the thickness of cell boundaries for the two magnets, the thickness of cell boundary is in the range of 7-15 nm for the type-A magnet, while the type-B magnet show the homogenous and stability phenomenon with wider thickness of cell boundaries (~15- 20 nm). Therefore, it is thought to account for the type-B magnet, a uniform continuous cellular structure with the smaller cell size and the homogeneous cell boundary phase will lead to the increase in the magnetocrystalline anisotropy energy fluctuations between the 2:17R cell and 1:5H cell boundary phase [13], which could lead to the enhancement of the magnetic properties of the $Sm_2Co_{17}$ alloy. Similar results were also observed previously in $(SmGdDy)(Co, Fe, Cu, Zr)_z$ [14], $Sm_2Fe_{17}$ [15] and $Sm_2Co_{17}$ [16] magnets. To gain further insight into the relation between the magnetic properties and the microstructures, we have tried to get the lattice constant from the SAED patterns.
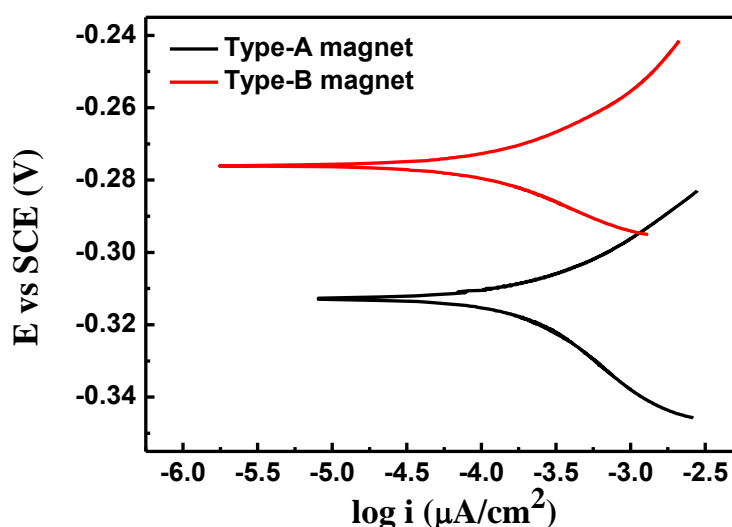


**Figure 5.** Polarization curves of the type-A and type-B magnets tested in 2.5 wt.% NaCl aqueous solutions.

As shown in Fig. 4 (c), the distance of OA can be measured by using the Digital Micrograph software, $R_1(OA)=2.3356$ nm$^{-1}$. The d-spacing of (110) and the lattice constant can be determined as below, respectively:

$$d_{(110)} = 1/R_1(OA) = (1/2.3356(1/nm)) = 4.2816\text{Å} \quad (1)$$

$$a = d_{(110)} \times 2 = 8.5632\text{Å} \quad (2)$$

So the calculated lattice constant α is 8.5632Å for the type-A magnet. Similarly, the lattice constant α of the type-B magnet is calculated in the same way about 8.6892Å. Therefore, it indicates that the different lattice constant α is one of the factors that enhancing the magnetic properties for the magnets made of jet-milling. Fig. 5 shows the potentiodynamic polarization curves for the type-A and type-B magnets tested in 2.5 wt.% NaCl aqueous solutions. The corresponding corrosion potential $E_{corr}$, corrosion current density $i_{corr}$ and Tafel slope $b$ were obtained and illustrated in Table 1. The corrosion current density of the type-A magnet is 112.20 μA/cm$^2$ derived from Tafel curve and the corrosion potential is -0.313 V, while the corrosion current density decreases to 31.62 μA/cm$^2$ and the corrosion potential increases to -0.276 V for the type-B magnet. Meanwhile, compared with the type-A magnet, the Tafel slope $b$ is also decreased from 138 mV/dec to 116 mV/dec. The higher value of corrosion potential $E_{corr}$ and lower value of corrosion current density $i_{corr}$ and Tafel slope $b$ for the type-B magnet means that the magnets made of jet-milling can remarkably improve the electrochemical stability and corrosion resistance in salt solution.

**Table 1.** The corrosion potential $E_{corr}$, corrosion current density $i_{corr}$ and Tafel slope $b$ of the type-A and type-B magnets tested in 2.5 wt.% NaCl aqueous solutions.

| Alloys | $E_{corr}$(V) | $i_{corr}$(μA/cm$^2$) | $b$(mV/dec) |
|--------|---------------|------------------------|-------------|
| Type-A | -0.313 | 112.20 | 138 |
| Type-B | -0.276 | 31.62 | 116 |
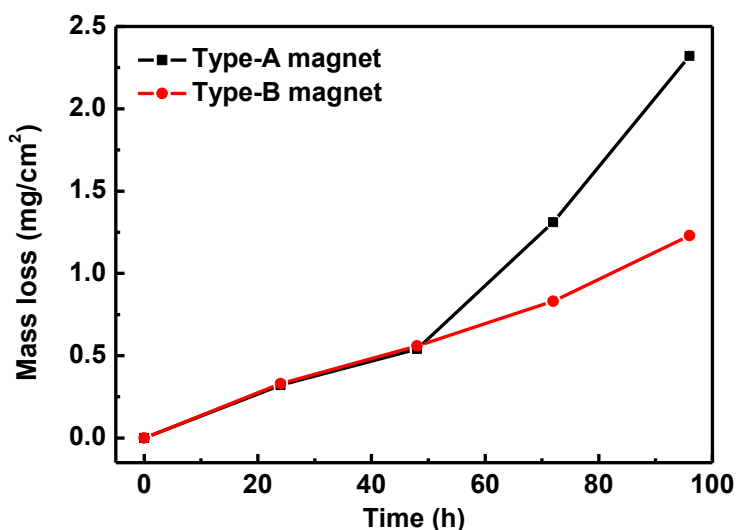


**Figure 6.** Mass loss of the type-A and type-B magnets measured in 120°C, 2 bar and 100% relative humidity atmosphere for different times.

The improvement of the corrosion resistance for the type-B magnet made of jet-milling is also reflected by the mass loss tests in hot and humid atmosphere, as shown in Fig. 6 for the magnets measured in 120°C, 2 bar and 100% relative humidity atmosphere for different times. It can be seen that the two samples have a nearly negligible mass loss of ~0.5 mg/cm$^2$ before 48 h. As the exposure time was further prolonged to 96 h, the mass loss of the type-B magnet reaches to ~1.2 mg/cm$^2$, compared to the type-A magnet with the mass loss increase to ~2.3 mg/cm$^2$. That means the corrosion resistance of the type-B magnet can be improved in hot/humid atmosphere, which may be attributed to the homogeneous cell boundary phase, similar to the reported results for the $SmCo_7$ magnets with Zr and Si co-substitution for more homogeneous microstructure [17]. It is held that the difference of microstructure and lattice constant are the primary reason that cause about such a huge difference on the magnetic properties and corrosion resistance behavior of the type-A and type-B magnets [18,19].

The present study demonstrated that the type-B magnet made by jet-milling can reduce the average cell size and improve the magnetic properties at the room/high temperature, which is believed to be a great potential hard magnet for high temperature applications. Meanwhile, the corrosion resistance of these magnets can be also improved.

## 4. CONCLUSION

The magnetic properties and the microstructures of the magnets were made of by ball-milling and jet-milling with the nominal composition $Sm(Co_{bal}Fe_{0.125}Cu_{0.08}Zr_{0.06})_{7.4}$ have been investigated. The corrosion resistance of the $Sm_2Co_{17}$ magnet made of jet-milling obtains uniform continuous cellular structure with the smaller cell size and the homogeneous cell boundary phase, which led to the improve of magnetic properties at the room/high temperature. Meanwhile, the corrosion resistance of these magnets can be also improved, with the lower corrosion current density $i_{corr}$ (31.62 µA/cm$^2$) and higher corrosion potential $E_{corr}$ (-0.276 V).

**Reference**

1. I. Panagiotopoulos, M. Gjoka, D. Niarchos, *J. Magn. Magn. Mater.,* 279 (2006) 389.
2. T. Matthias, G. Zehetner, J. Fidler, W. Scholz, T. Schrefl, D. Schobinger, G. Martinek, *J. Magn. Magn. Mater.,* 242 (2002) 1353.
3. D. Goll, H. Kronmüller, H.H. Stadelmaier, *J. Appl. Phys.,* 96 (2004) 6534.
4. X. Wang, X. Peng, H. Zhao, Zh. Guo, W. Li, F. Wang, *J. Appl. Phys.,* 117 (2015) 093902.
5. L. Rabenberg, R. K. Mishra, G. Thomas, *J. Appl. Phys.,* 53 (1982) 2389.
6. X.Y. Xiong, T. Ohkubo, T. Koyama, K. Ohashi, Y. Tawara, K. Hono, *Acta Mater.,* 52 (2004) 737.
7. O. Gutfleisch, K.H. Müller, K. Khlopkov, M. Wolf, A. Yan, R. Schäfer, T. Gemming, L. Schultz, *Acta Mater.,* 54 (2006) 997.
8. J.F. Liu, Y. Ding, G.C. Hadjipanayis, *J. Appl. Phys.,* 85 (1999) 1670.

9.  T.G. Woodcock, O. Gutfleisch, *Acta Mater.*, 59 (2011) 1026.
10. W.F. Li, T. Ohkubo, K. Hono, *Acta Mater.*, 57 (2009) 1337.
11. Tae-Hoon Kim, Seong-Rae Lee, Min-Woo Lee, Tae-Suk Jang, Jin Woo Kim, Young Do Kim, Hyo-Jun Kim, *Acta Mater.*, 66 (2014) 12.
12. M.X. Pan, P.Y. Zhang, H.L. Ge, Q. Wu, *Mater. Technol.*, 31 (2016) 580.
13. W. Sun, M.G. Zhu, Z.H. Guo, Y.K. Fang, W. Li, *Physica B.,* 476 (2015) 154.
14. L. Liu, D. L. Pan, Z. Liu, H.W. Zhang, M. Li, R.J. Chen, X.M. Liu, A.R. Yan, D. Lee, W. Li, *J. Magn. Magn. Mater.*, 374 (2015) 634.
15. L.X. Zhao, L.Y. Zheng, G.C. Hadjipanayis, *Funct. Mater. Lett.,* 6 (2013) 1350038.
16. N.J. Yu, M.G. Zhu, L.W. Song, Y.K. Fang, K.K. Song, Q. Wang, W. Li, *J. Magn. Magn. Mater.,* 452 (2018) 272.
17. D.Y. Feng, Z.W. Liu, G. Wang, Z.G. Zheng, D.C. Zeng, Z. Li, G.Q. Zhang, *J. Alloys Compd.*, 610 (2014) 341.
18. J.L. Xu, Q.F. Xiao, D.D. Mei, Y.X. Tong, Y.F. Zheng, L. Li, Z.C. Zhong, *Surf. Coat. Tech.,* 309 (2017) 621.
19. W. Sun, M.G. Zhu, Y.K. Fang, Z.Y. Liu, H.S. Chen, Z.H. Guo, W. Li, *J. Magn. Magn. Mater.,* 378 (2015) 214.